Journal of Water Resource and Protection, 2026, 18(11), 743-768
https://www.scirp.org/journal/jwarp
ISSN Online: 1945-3108
ISSN Print: 1945-3094

Study of the Spatio-Temporal Variation of Artisanal Gold Mining Using Machine Learning Algorithms in the Upper N'ZI Watershed (North-Central Côte d'Ivoire)

Yao Amonkonan Jean-Philippe Bene[1], Kouassi Ernest Ahoussi[2], Kouassi Serge Aristide Yao[3], Armand Patrick Yapo[2]

[1]École Doctorale Sciences Technologie et Agriculture Durable (ED-STAD), Université Félix Houphouët Boigny, Abidjan, Côte d'Ivoire
[2]Laboratoire des Sciences du Sol, de l'Eau et des Géomateriaux (LSSEG)/UFR des Sciences de la Terre et des Ressources Minières (STRM)/Université Felix Houphouët Boigny, Abidjan, Côte d'Ivoire
[3]Laboratoire de Géographie Physique, UFR Communication et Société (CS), Université Alassane Ouattara, Bouaké, Côte d'Ivoire
Email: beneyaoa5@gmail.com, akouassiernest@gmail.com, armandpatrickyapo@gmail.com, yyserge0@gmail.com

How to cite this paper: Bene, Y.A.J.-P., Ahoussi, K.E., Yao, K.S.A. and Yapo, A.P. (2026) Study of the Spatio-Temporal Variation of Artisanal Gold Mining Using Machine Learning Algorithms in the Upper N'ZI Watershed (North-Central Côte d'Ivoire). *Journal of Water Resource and Protection*, **18**, 743-768.
https://doi.org/10.4236/jwarp.2026.1811037

Received: September 13, 2026
Accepted: November 15, 2026
Published: November 18, 2026

Copyright © 2026 by author(s) and Scientific Research Publishing Inc.
This work is licensed under the Creative Commons Attribution International License (CC BY 4.0).
http://creativecommons.org/licenses/by/4.0/
Open Access

Abstract

Located in north-central Côte d'Ivoire, the Upper N'ZI watershed (BVHN) is experiencing an intensification of artisanal gold mining, placing significant pressure on the environment and natural resources. This study aims to analyze the impact of this activity on land-cover changes between 2017 and 2024. Sentinel-2A images were processed using Random Forest (RF) machine learning algorithms implemented on Google Earth Engine via *JavaScript* programming. Validation of the resulting classifications yielded overall accuracies of 89.97% (2017) and 87.28% (2024), with Kappa coefficients of 0.85 and 0.84 for the respective years. The results reveal a marked decline in natural land cover, such as open forests (−18.14%), dense forests (−26.15%), and water bodies (−37.54%). Conversely, the study shows a significant increase in the effects of human activity, particularly regarding artisanal gold mining sites (+117.66%), built-up areas/bare soil (+22.49%), croplands (+0.62%), and wooded savannas (+20.02%). This trend driven by agricultural expansion, urban development, and the intensification of artisanal mining is significant. Post-classification change analysis further highlights a predominant conversion of wooded savanna and cropland classes as well as the other four land-cover classes into artisanal gold mining sites. Furthermore, it reveals a progressive decline in the water retention coefficient over the study period likely attributable to the gradual anthropization of the Upper N'ZI watershed which could exacerbate ero-

sion risks. The study therefore calls for sustainable resource management to reconcile local development with environmental preservation.

Keywords

Artisanal Gold Mining, Land Use, Job-to-Classification Comparison, Google Earth Engine, Upper N'ZI Watershed, Côte d'Ivoire

1. Introduction

In many traditional African societies, the possession of gold, a precious metal, was motivated by the various socio-cultural functions it played. Gold found in nature was not to be sold, as it was considered a gift from deities and spirits and, therefore, remained intimately linked to the soul, fortune, and destiny of the finder [1]. Today, the social and symbolic functions that gold played in traditional Ivorian societies, and which justified its acquisition, seem to have disappeared in the quest for this precious metal. Indeed, artisanal gold mining appears to be motivated by the search for significant and rapid personal financial gain [2]. In this regard, recent data from a 2023 study by the NGO [3] show that the proliferation of gold panning sites is rapidly expanding, affecting most regions and involving more than 500,000 people in rural areas, as described in the report and in the work of [4]. The gold rush has gripped the entire country, increasingly fueling the greed of many individuals from all walks of life. While perceived by some as an economic driver, it generates numerous negative impacts, particularly on the environment (deforestation, pollution, soil and water degradation) and on the socio-cultural level (moral depravity, gender-based violence, threats to archaeological sites) [5]-[8]. In reality, artisanal gold mining generates numerous environmental problems, such as landscape shaping, deforestation, biodiversity loss, air pollution, soil and water resource degradation, etc. [9]. Furthermore, from a socio-cultural perspective, the work of [10] showed that gold panning is a major threat to archaeological sites in certain areas of Côte d'Ivoire. Most of the significant work on mapping gold panning sites has focused on the spatiotemporal dynamics of land cover in several regions of Côte d'Ivoire. However, no study has been conducted on the spatiotemporal contribution of gold panning sites to land cover dynamics in the BVHN. It is from this perspective that the study was initiated to identify the contribution of gold panning activities to the degradation and modification of natural resources in the environment of the upper N'ZI watershed. The objective of the study is therefore to assess the impact of gold panning on changes in land use in the upper N'ZI watershed.

2. Description of the Study Area

The study area is the Upper N'ZI Watershed (BVHN), a sub-watershed of the N'ZI River as illustrated in **Figure 1**. It lies between longitudes 4˚50'00" and 5˚22'00"

West, and latitudes 7˚40'00" and 9˚26'00" North, and covers an area of approximately 8794 km^2. It originates in northern Côte d'Ivoire, in the Tchologo region, at an altitude of 400 m, and flows in a north-south direction. The BVHN partially covers the departments of Ferkessédougou, Kong, Niakaramadougou, Katiola, Dabakala, and Bouaké. It is characterized by a Sudanese climate, with a rainy season from April to October and a dry season from November to March, exacerbated by the Harmattan wind. Average annual rainfall is less than 1200 mm and the average temperature is 26.7˚C. The basin is generally characterized by a rather monotonous landscape [11], with elevations ranging from 300 m in the south to 400 m in the north. The Sudanian zone to which the study area belongs is characterized by shrubby or herbaceous savanna, wooded savanna, and forested savanna vegetation. Alongside this savanna vegetation, patches of degraded forest and gallery forests are observed. The soil characteristics of the BVHN are dominated by ferralsols [12] [13]. The geology of the basin is characterized by formations of true calc-alkaline Eburnean granitic types or various "Baoulé" granites (muscovite granites, two-mica granites, amphibolite-biotite granites, and granodiorites). The aquifers encountered are those of the weathered rocks and the basement (fissured and fractured). The main activity, which is also the primary source of income for the population, is agriculture, consisting of cotton, yams, irrigated rice, and citrus fruits.

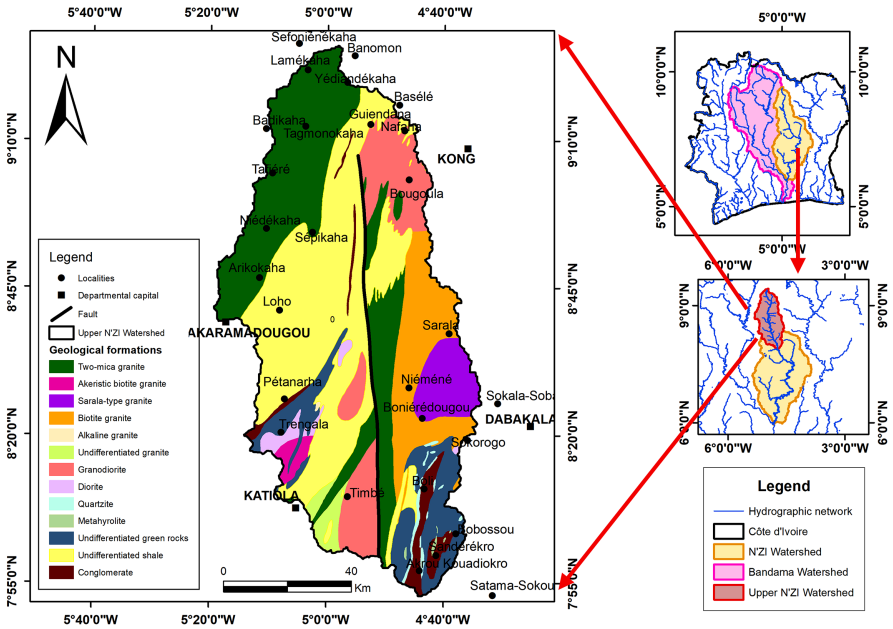


Figure 1. Location map of the upper N'ZI watershed.

3. Materials and Methods

3.1. Materials and Data Used

The characterization of land cover units on the Google Earth Engine (GEE) platform required the use of 10 m resolution Sentinel-2A multispectral satellite images from the years 2017 and 2024. The images come from archived GEE data

offering the best quality and the lowest possible level of cloud cover (≈ 0%). Four (04) scenes covering the study area were selected. Only the seven multispectral bands (B2 (Blue), B3 (Green), B4 (Red), B8 (PIR), B8A (PIR2), B11 (SWIR 1) and B12 (SWIR 2)) (Table 1). The mapping of land cover units was carried out using the *JavaScript* programming language using the Google Earth Engine Editor Code and its web cartographic libraries.

Table 1. Characteristics of the Sentinel-2A images of the study area.

Scenes from Sentinel-2A		Spectral channel	Spatial resolution	Spectral range
2017	2024			
T30PUQ on 03/11/2017 T30PTR on 29/12/2017 T30NTP on 24/12/2017 T30PUR on 03/11/2017	T30PTQ on 02/01/2024 T30PUR on 22/02/2024 T30NTP on 14/01/2024 T30PUQ on 27/01/2024	B2 (Bleu)	10 m	0.46 - 0.52 µm
		B3 (Vert)	10 m	0.54 - 0.58 µm
		B4 (Rouge)	10 m	0.65 - 0.68 µm
		B8 (PIR)	10 m	0.78 - 0.90 µm
		B8A (PIR2)	20 m	0.85 - 0.87 µm
		B11 (SWIR 1)	20 m	1.57 - 1.66 µm
		B12 (SWIR 2)	20 m	2.10 - 2.28 µm

3.2. Methodology

3.2.1. Image Selection

The first step in studying land cover dynamics using Google Earth Engine (GEE) is collecting the images to be used. This involves imposing conditions on variables such as the boundaries of the study area, the type of satellite image, the study period, cloud cover, and the wavelength of the bands.

- The condition on the location of the images was imposed by the boundary of the BVHN, the subject of this study, which was imported into the GEE environment from the «Table Upload» tool of the Asset module. Then the extraction of the portions covered by the boundary of the area, on the resulting collection was carried out using the clip() command.
- The product type requirement was met by selecting Sentinel-2 surface reflectance (BOA) images. Level 2A images were used. These images are already geometrically, radiometrically, and atmospherically corrected by the supplier. In the GEE work interface, the Level 2A Sentinel-2 images were imported using the ee.ImageCollection (COPERNICUS/S2_SR) command.
- The condition on the period was set, ranging from January 1st to December 31st for the years 2017 and 2024 in GEE using the filterDate (start, end) command.
- The cloud cover condition was met by imposing a cloud cover threshold value of 1% or less to ensure data was available for the entire area. The cloud pixel percentage value, stored as metadata for each image, was used to select and extract only the images with 0% cloud cover in the study area, using the filterMe-

tadata ('CLOUD_COVERAGE_ASSESSMENT') command.

- Finally, the selection of the bands to be used was based on the spectral resolution (wavelength) and spatial resolution (value of the smallest ground pixel) of the different bands. Applying a filter to extract only the multispectral bands resampled to a spatial resolution of 10 m (B2 (Blue), B3 (Green), B4 (Red), B8 (NIR), B8A (NIR2), B11 (SWIR 1), and B12 (SWIR 2)) is considered more than sufficient for identifying land-cover units in the study area, using the select (band) command. This filter is considered more than sufficient to identify the land cover units in the study area using the «select(band)» command. These images, preprocessed from Google Earth, are then used to map land cover using machine learning algorithms (AML). Figure 2 shows the images resulting from this processing within the context of this study.



Figure 2. Raw Sentinel-2 images from 2024.

3.2.2. Preparation of Input Data

Spectral indices are essential parameters that highlight key image information, providing a generalized view of different land cover units to facilitate sampling of areas of interest.

To better distinguish between different types of land cover units, appropriate spectral indices have been calculated. The importance of these spectral indices in identifying areas of interest in mapping has been demonstrated in several recent studies, including: [14]-[22]. The main indices used in this study are listed below:

- Normalized Difference Vegetation Index: $\mathrm{NDVI} = \frac{(\mathrm{NIR} - \mathrm{RED})}{(\mathrm{NIR} + \mathrm{RED})}$;
- Ground-Adjusted Vegetation Index: $\mathrm{SAVI} = \frac{(\mathrm{NIR} - \mathrm{RED})}{(\mathrm{NIR} + \mathrm{RED} + L)} \times (1 + L)$ With $L = 0.5$;

- Normalized Difference Water Index: $\mathrm{NDWI} = \frac{(\mathrm{NIR} - \mathrm{SWIR})}{(\mathrm{NIR} + \mathrm{SWIR})}$;
- Modified Normalized Difference Water Index: $\mathrm{MNDWI} = \frac{(\mathrm{GREEN} - \mathrm{SWIR})}{(\mathrm{GREEN} + \mathrm{SWIR})}$;
- Urbanization Index by Standardized Difference: $\mathrm{NBRI} = \frac{(\mathrm{NIR} - \mathrm{SWIR1})}{(\mathrm{NIR} + \mathrm{SWIR1})}$;
- Brightness Index: $\mathrm{IB} = \sqrt{\mathrm{NIR}^2 + \mathrm{RED}^2}$.

The spectral indices are then displayed in the GEE interface as images generated from the various calculation operations. These index layers allow for the identification of different land cover units, thus increasing the accuracy of the classification [20]. To carry out this operation, the use of high-resolution Sentinel-2A images at the boundaries of the study area proved essential. Using these images, a layer was generated for each of the calculated indices (NDVI, SAVI, NDWI, MNDWI, NBRI, and IB).

3.2.3. Resampling and Normalization of Spectral Bands

To harmonize image spatial resolution and integrate 20 m bands with native 10 m bands, spectral bands originally acquired at 20 m resolution were resampled to 10 m using bilinear interpolation. This preprocessing step enabled the sampling of all training plots at a 10 m resolution prior to training the supervised classification model. This methodology has been employed in previous studies, such as [23] and [24].

Normalization, for its part, consists of standardizing the intrinsic characteristics of the bands by placing them within the same value range, with the aim of harmonizing the values of the different bands of an image [20]. In this study, normalization was limited to reducing variations in brightness and contrast between bands to facilitate analysis and information extraction. This results in a more consistent and balanced representation of the information contained in each band, thus facilitating subsequent analyses such as classification, change detection, and feature extraction.

3.2.4. Selection of Land-Cover Units, Training Points, and Classification Units

To perform supervised image classification on the GEE platform, it is first necessary to define sampling areas representing the various land-cover classes to be identified [25]. In this study, field knowledge, combined with calculated index layers, enabled the selection of training plots. A total of seven land-cover classes within the study area were selected dense forest, open forest, wooded savanna, cropland, built-up areas/bare soil, artisanal mining sites, and water and are defined in **Table 2** below.

The classification method used is pixel-based; consequently, the control points (training and validation) represent the classes to which they belong, thereby avoiding issues associated with mixed pixels. During the learning process, the collected samples are split into training and validation datasets. Using the GEE 'ran-

domColumn' function, the dataset is subdivided by assigning a random value to each sampling point. With these random values ranging from 0 to 1, 70% of the samples are selected for the training dataset using the command 'ee.Filter.lt('random', 0.7)', while the remaining 30% are used for the validation dataset via the command 'ee.Filter.gte('random', 0.7)'. Once trained, the model is applied to classify the image pixels and generate a classification map. Table 3 below presents the number of samples collected per land-cover unit for each year.

Table 2. Description of the different land-use units.

N°	Class	Description
1	Dense forest	Thick, continuous plant cover, with little clear ground space.
2	Open forest	Vegetation consisting of widely spaced trees, with some grasses allowing light to reach the ground.
3	Wooded savanna	Vegetation consisting of scattered trees and shrubs interspersed with grasses and bushes, creating an open, unobstructed landscape.
4	Culture	Area comprising various plantations such as maize, cotton, sorghum, cashew, rubber, palm, cocoa, and others.
5	Built-up Area/Bare Soil	Urbanized areas, roads, areas devoid of vegetation, and gold mining areas.
6	Gold panning site	Site on which the activity is carried out or which has experienced gold mining and which sometimes houses the actors.
7	Water	Class comprising watercourses and water reservoirs.

Table 3. Number of samples per land-cover unit.

Class	Codification	Number of samples	
		2017	2024
Dense forest	FD	32	27
Open forest	FC	54	30
Wooded savanna	SA	72	42
Culture	Cu	70	35
Built-up Area/Bare Soil	BSn	37	50
Gold panning site	Or	30	37
Water	Ea	33	27

To validate the control points, a field data collection campaign was conducted from March 7 to 15, 2025, covering 15 sites selected based on accessibility. Overall, these sites exhibit characteristics representative of the land-cover units considered in this study. Figure 3 illustrates the distribution of the field data collection sites.

The campaign enabled the recording of geographic coordinates and precise descriptions of the verified land-cover units, thereby strengthening the validation

process. Following this field campaign, each homogeneous 10-meter ground unit was assigned a corresponding reference land-cover unit based on the Sentinel-2 imagery. Comparing the field observations with the pre-processed 2024 reference image allowed for the validation of the classification. Table 4 below illustrates this methodology.

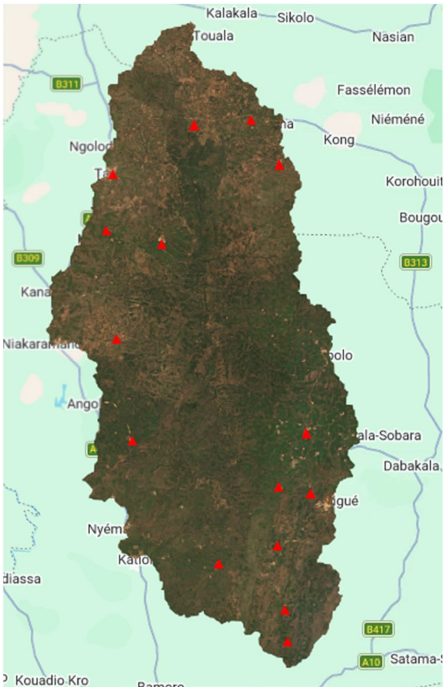
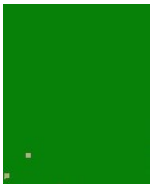
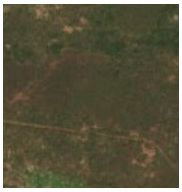
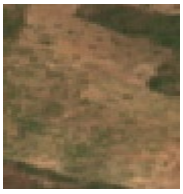
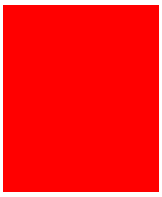
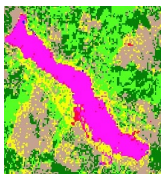
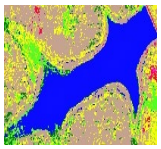


Figure 3. Field data collection site (Ground truth).

Table 4. Validation of land-cover units.

Class	Geographic coordinates	Sentinel-2 image	OCS	Photography
Dense forest	8˚30'59.02"N 4˚51'22.35"O			
Open forest	8˚12'13.59"N 4˚42'30.31"O			
Wooded savanna	9˚17'31.73"N 4˚59'37.50"O			

续表

Culture	9˚8'51.77"N 4˚56'21.34"O			
Built-up Area/Bare Soil	9˚4'11.48"N 5˚9'44.72"O			
Gold panning site	8˚30'47.62"N 5˚9'15.73"O			
Water	8˚3'59.53"N 4˚58'8.09"O			

3.2.5. Supervised Classification Methodology and Evaluation

The supervised classification performed using the Random Forest (RF) machine learning algorithm implemented on the GEE platform is the one employed in this study. This methodology has been successfully applied by numerous authors including [20] [26]-[28] to map land-cover units in Iran, the Czech Republic, Morocco, and Côte d'Ivoire, respectively. This non-parametric classifier relies on aggregating the results from an ensemble of decision trees built using random subsets of observations and explanatory variables. In this study, the model was trained on 328 samples for the 2017 imagery and 248 samples for the 2024 imagery, distributed across seven classes (FD, FC, SA, Cu, BSn, Or, Ea). Training utilized 13 explanatory variables, comprising seven Sentinel-2 spectral bands (B2, B3, B4, B8, B8A, B11, and B12) and six spectral indices (NDVI, SAVI, NDWI, MNDWI, NBRI, and IB). Key model hyperparameters specifically the number of trees, the number of variables considered at each split node, the minimum number of samples per leaf, and the sampling fraction were tuned to achieve a stable and high-performing classification.

Evaluating the classification methodology begins with analyzing the model's performance and accuracy by comparing the classification results with independent validation data (e.g., sampling points not used for training). Next, calculating the Kapa coefficient and using metrics such as the confusion matrix, overall accuracy, and accuracy per class are statistical tools for evaluating the classification. This analysis quantifies the model's performance and identifies potential errors or

biases in the classification, thus providing a detailed assessment of the quality of the results obtained [20] [29].

- Confusion matrix

The confusion matrix, sometimes referred to as the error matrix, is an essential method for evaluating the accuracy of land cover. It plays a central role in most accuracy assessments of thematic maps [30]. In this study, the confusion matrix was generated from GEE using the command code «ee.Classifier.confusionMatrix()».

- Précision du producteur (PP)

Producer's accuracy is the probability that a pixel of a given class X in the field is correctly classified in class X on the map [20] [29]. The function «confusionMatrix().producersAccuracy()» was used to determine the producer's accuracy of the different classifications for the two periods studied.

- Précision de l'utilisateur (PU)

User accuracy is the probability that a pixel classified as X on the map belongs to X on the ground [20] [29]. The algorithm «confusionMatrix().consumersAccuracy()» was used to determine the user accuracy of the different classifications for the two periods studied.

- Précision globale (PG)

Overall accuracy reflects the proportion of correctly classified test data and is the most commonly used measure for evaluating the efficiency and accuracy of classifiers [29]. It was automatically generated from GEE using the command «confusionMatrix().accuracy()».

- Coefficient de Kappa (K)

The Kappa coefficient is a measure of accuracy that ranges from 0 to 1. According to [31], it assesses the agreement between the classified map and the actual field data by using all the elements of the confusion matrix, not just those located on the diagonal. The algorithm «confusion Matrix().kappa()» generates the Kappa coefficient for different classifications.

The work of Landi and al. in 1977, cited by [32], classified the Kappa coefficient into a range of five qualitative categories from poor to excellent. **Table 5** below presents this scale.

Table 5. Agreement based on the Kappa coefficient.

K	Concordance of results
[−1.00; 0.20]	Bad
[0.21; 0.40]	Low
[0.41; 0.60]	Moderate
[0.61; 0.80]	Good
[0.81; 1.00]	Excellent

3.3. Assessment of Land Use Trends

3.3.1. Average Annual Spatial Expansion Rate (T)

In order to analyze land-use dynamics, it was necessary to calculate the average annual rate of spatial expansion. This rate of change is estimated using [33] formula, commonly employed to measure the growth of macroeconomic aggregates between two given periods. This formula is presented as follows (Equation 2):

$$T = \frac{\ln V_{i1} - \ln V_{i0}}{(t_1 - t_0) \times \ln e} \times 100 \quad (1)$$

with: T = Annual rate of spatial expansion; V_{i0} = Proportion of unit i of land cover taken in the initial state; V_{i1} = Proportion of unit i of land cover taken in the final state; i = the unit or class of land cover considered; t_0 = the initial year of the period considered; t_1 = the final year of the period considered; ln = natural logarithm; e = base of the natural logarithm (e = 2.71828).

3.3.2. Overall Rate of Change in Land Cover Classes (TG)

The TG allows us to estimate the proportion of gain or loss in area for different land cover units. Analysis of the rate of change values shows that positive values indicate progression, while negative values signal regression. Values close to zero suggest that the class is relatively stable. The formula used for this calculation is described in the study by [31], represented here by Equation 2.

$$T_G = \frac{(V_{i1} - V_{i0})}{V_{i0}} \times 100 \quad (2)$$

where: T_G = Average annual rate of change of land cover unit i; V_{i0} = Proportion of land cover unit i in its initial state; V_{i1} = Proportion of land cover unit i in its final state; i = the land cover unit or class considered.

3.3.3. Assessment of the Conversion of Land-Use Classes into Artisanal Gold Mining Sites between 2017 and 2024

A post-classification transition analysis was conducted in GEE using JavaScript programming to identify land-cover changes between 2017 and 2024, applying the method developed by [34]. The two previously classified maps were cross-tabulated on a pixel-by-pixel basis to generate a transition matrix from the initial classes (2017) to the final artisanal gold mining site class (2024). A targeted analysis of pixels classified as artisanal gold mining sites in 2024 subsequently made it possible to identify their original land-cover category in 2017 and quantify the corresponding proportions [35]. Transition areas were calculated based on the number of 10-meter resolution pixels and expressed in both square kilometers and percentages. This approach thus enables the identification of the primary land-cover classes that contributed to the expansion of gold mining activities in the BVHN between 2017 and 2024 [36].

3.3.4. Water Retention Capacity Index for Land Use Types

One of the direct consequences of land use on surface water resources is anthropization. The water retention coefficient, which varies according to the type of land

use, makes it possible to assess the impact of different land-use units on the basin's surface runoff. The water retention capacity index (C_r) is calculated using the equation proposed by [37], which has been adopted in several other studies on land-use dynamics [38]-[41].

$$C_{ri} = \sum_i P_i \times a_i \quad (3)$$

with C_{ri} = Water retention capacity of land cover class I; P_i = Percentage of the total area of the study area occupied by land cover unit i; a_i = Weighting coefficient which indicates the effective water retention capacity of land cover unit i.

For each land-use type, the coefficient "a_i" ranges from 0 to 2. A value of zero signifies "zero reduction in retention," while a value of two indicates "maximum reduction in retention" [37] [40]. Thus, following the work of [37], a value of 2 was assigned to the dense forest and open forest classes due to their significant vegetation cover, which considerably reduces runoff intensity. An intermediate value of 1 was assigned to the wooded savanna and cultivated land classes. A low value of 0.5 was assigned to the artisanal gold mining sites class, accounting for the residual vegetation sometimes found there and the fact that extraction occurs beneath the vegetation cover. Finally, a value of 0 was assigned to the settlement and bare soil classes. The methodology aims to measure a terrestrial environment's capacity to retain water following precipitation; this objective drove the decision to exclude the water class, as it already constitutes a water reservoir.

4. Results and Discussion

4.1. Classification Evaluation Results

The processing and classification performed using the RF Machine Learning algorithm implemented on the Google Earth Engine (GEE) platform enabled the precise identification of seven (7) classes and the mapping of land cover in the study area for 2017 and 2024. The results of this classification were then evaluated using PP, PU, PG, K analysis and a confusion matrix.

4.1.1. Classification of Sentinel-2 Images from 2017

The overall accuracy and Kappa values are 89.96% and 0.86, respectively. The results for Producer Accuracy (PP) and User Accuracy (PU) are recorded in **Table 6** below:

Table 6. Clarification from the producer and user regarding the 2017 classification.

Settings	Land use units						
	Dense Forest	Open Forest	Wooded savanna	Culture	Built-up Area/Bare Soil	Gold Panning Sites	Water
PP (%)	98.00	95.00	91.00	56.00	90.00	87.00	95.00
PU (%)	99.00	95.00	90.00	56.00	93.00	78.00	99.00

Producer accuracy (PP) values range from 56% to 98%. The highest values are

observed in pixels classified as dense forest and water, while the lowest corresponds to the crop class. The same pattern holds true for user accuracy (PU), except that for this parameter, the highest value is 99% and the lowest is 56% for the same classes as PP (See Figure 4).

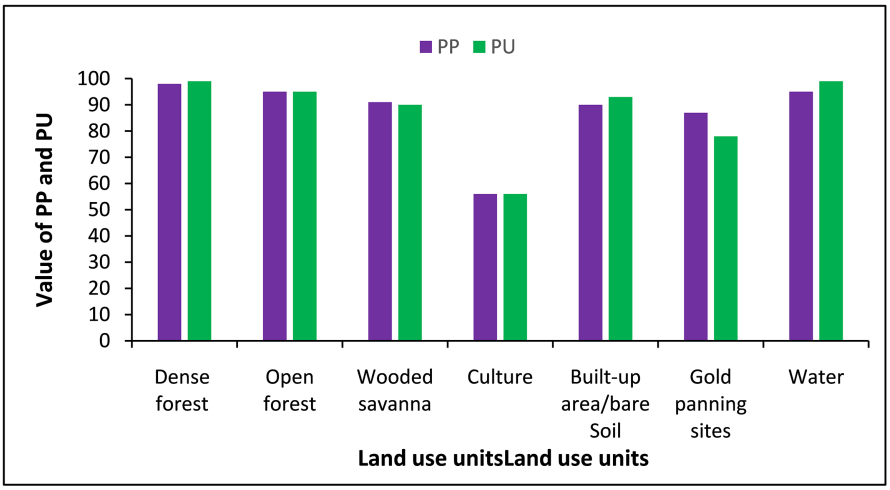


Figure 4. Clarification from the producer and user regarding the 2017 classification.

Table 7 lists the errors that may have occurred during data processing:

Table 7. Confusion matrix for the 2017 classification.

Classes	Dense Forest	Open Forest	Wooded savanna	Culture	Built-up Area/Bare Soil	Gold Panning Sites	Water
Dense Forest	97.82	1.49	0.00	0.30	0.00	0.00	0.00
Open Forest	1.96	96.19	0.08	1.67	0.00	0.00	0.00
Wooded savanna	0.22	0.58	97.19	1.78	0.80	0.00	0.00
Culture	0.00	1.74	2.13	95.19	0.15	0.82	0.00
Built-up Area/Bare Soil	0.00	0.00	0.46	0.03	97.03	2.68	0.00
Gold Panning Sites	0.00	0.00	0.00	0.70	1.80	95.18	1.00
Water	0.00	0.00	0.14	0.33	0.22	1.32	99
TOTAL	100	100	100	100	0.00	100	100

Analysis of the confusion matrix shows good classification of the different land cover units. Accuracy is 97.82% for the dense forest class, 96.19% for the open forest class, 95.19% for the cultivated land class, 96.03% for the built-up area/bare soil class, 94.58% for the gold mining site class, and 100% for the water class. However, some confusion is observed between the following classes:

- the dense forest class is identical to the open forest class by 1.96%;
- the open forest class coincides with the 1.74% cultivated class;
- the wooded savannah class coincides with the 2.13% cultivated class;

- the built-up area/bare soil class is identical to the gold panning site class of 1.80%;
- the gold panning sites class is indistinguishable from the water class of 1.32%.

4.1.2. Classification of Sentinel-2 Images from 2024

The results of the analysis of the classification of Sentinel-2 images from 2024 in the study area show an overall accuracy of PG = 87.17% and a Kappa coefficient of 0.84. The accuracy values for the producer and the user are presented in Table 8 below.

Table 8. 2024 Producer and user specifications.

Settings	Land use units						
	Dense Forest	Open Forest	Wooded savanna	Culture	Built-up Area/Bare Soil	Gold Panning Sites	Water
PP (%)	95.90	93.00	87.60	72.70	87.10	82.30	95.10
PU (%)	96.50	92.00	87.60	71.50	84.90	87.20	92.80

Regarding producer accuracy (PP), the 2024 image classification yielded satisfactory results, ranging from 72.70% for the crop class to 95.90% for the dense forest class. Similarly, for user accuracy (PU), the lowest value was for the crop class at 71.50%, and the highest was for the dense forest class at 96.50% (See Figure 5).

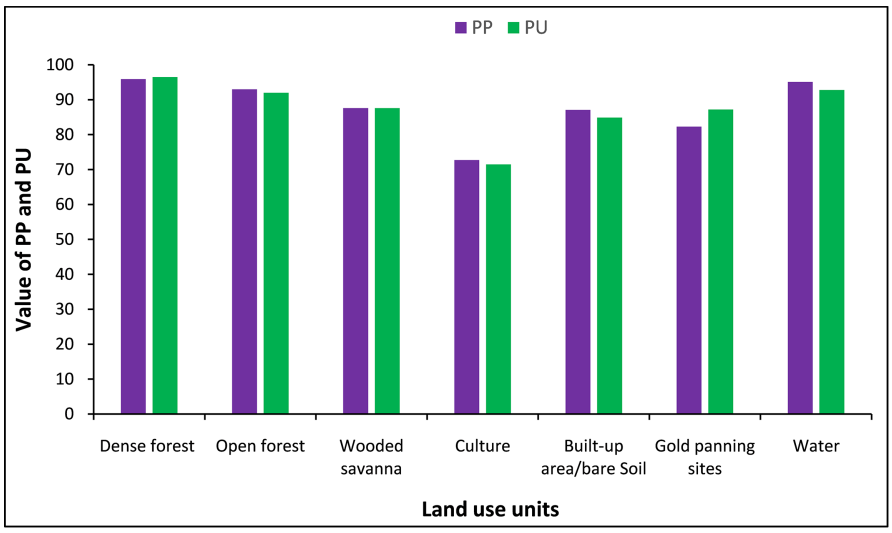


Figure 5. Clarification from the producer and user regarding the 2024 classification.

The confusion matrix of the different land cover units in the 2024 images is presented in Table 9 below.

Analysis of this table shows an acceptable classification of the different land cover units. Accuracy ranges from 95.49% for the cultivated land class to 98.78% for the water land class. Intermediate values are as follows: 95.61% for the wooded

savanna class, 97.04% for the open forest class, 97.21% for the gold mining site class, 97.92% for the built-up area/bare soil class, and finally 98.45% for the dense forest class. However, some slight confusion is noted between the following classes:

- the dense forest class is identical to the open forest class by 1.08%;
- the light forest class is identical to the 1.30% cultivated class;
- the wooded savannah class coincides with the 1.84% cultivated class;
- the built-up area/bare soil class is identical to the gold panning site class by 1.28%;
- the water class, is identical with the gold panning site class of 1.41%.

Table 9. Confusion matrix for the 2024 classification.

Classes	Dense Forest	Open Forest	Wooded savanna	Culture	Built-up Area/Bare Soil	Gold Panning Sites	Water
Dense Forest	98.45	1.44	0.08	0.21	0.00	0.00	0.00
Open Forest	1.08	97.04	0.54	1.26	0.00	0.00	0.00
Wooded savanna	0.31	0.22	95.61	1.51	0.14	0.39	0.00
Culture	0.15	1.30	1.84	95.49	0.66	0.39	0.00
Built-up Area/Bare Soil	0.00	0.00	0.90	0.89	97.92	1.63	0.00
Gold Panning Sites	0.00	0.00	0.82	0.64	1.28	97.21	1.41
Water	0.00	0.00	0.22	0.00	0.00	0.39	98.78
TOTAL	100	100	100	100	100	100	100

4.2. Assessment of the Dynamics of Land Cover Units between 2017 and 2024

4.2.1. Highlighting the Change

Quantitative analysis of maps derived from the classification of Sentinel-2 images from 2017 and 2024 highlights the spatial distribution of the seven (7) land cover units included in this study. Table 10 presents the proportion of land occupied by each class in the study area.

In 2017, the BVHN was dominated by the wooded savanna class, covering 3246.74 km^2 (36.92%), followed by the cultivated land class with 2000.63 km^2 (22.75%). Next came the open forest class, covering 1725.38 km^2 (19.2%), and the dense forest class, covering 1567.09 km^2 (17.82%). Then come the three other classes with the lowest proportions of built-up area to bare land (218.97 km^2, or 2.29%), the water class (20.22 km^2, or 0.23%), and the gold mining site class (14.95 km^2, or 0.17%).

In 2024, the wooded savanna class remains dominant with 3896.62 km^2, or 44.31%, followed by the cultivated land class at 2012.94 km^2, or 22.89%. Next come the intermediate classes: open forest with 1412.31 km^2, or 16.06%, and dense forest with 1157.29 km^2, or 13.16%. Finally, the classes with the smallest proportion are

the built-up area/bare soil class with an area of 268.21 km² or 3.05%, the gold mining site class with an area of 32.54 km² or 0.37% and the water class with an area of 12.63 km² or 0.16%.

Table 10. Percentage of classes.

Classes	Areas			
	2017		2024	
	km²	%	km²	%
Dense Forest	1567.09	17.82	1157.29	13.16
Open Forest	1725.38	19.62	1412.31	16.06
Wooded savanna	3246.74	36.92	3896.62	44.31
Culture	2000.63	22.75	2012.94	22.89
Built-up Area/Bare Soil	218.97	2.49	268.21	3.05
Gold Panning Sites	14.95	0.17	32.54	0.37
Water	20.22	0.23	12.63	0.16
Total	8794	100	8794	100

The maps in Figures 6-9 below allow for a quantitative assessment of the proportion of different land cover units from 2017 to 2024.

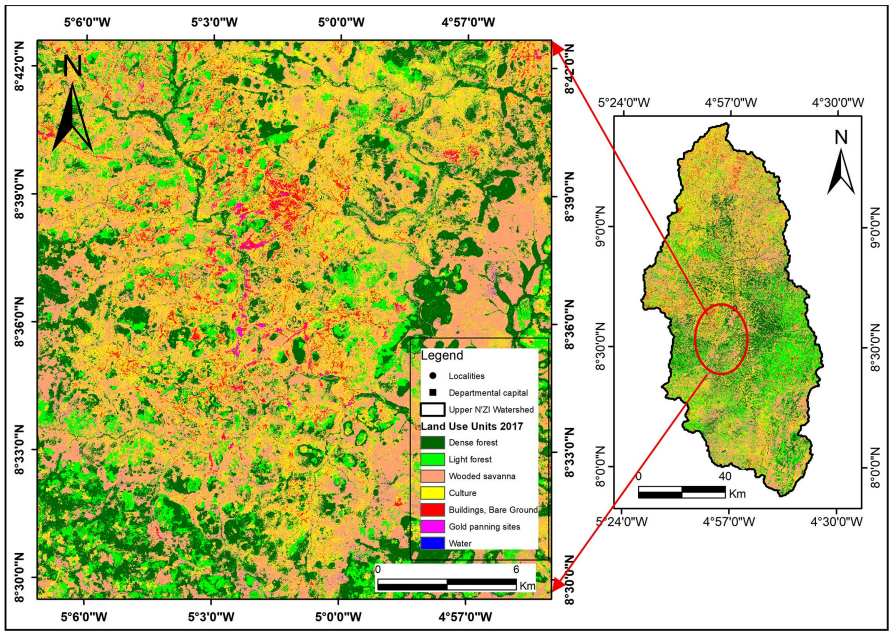


Figure 6. Land use in 2017 in the central-western region of the BVHN.

4.2.2. Assessment of the Evolution of Land Use Dynamics

The spatiotemporal evolution of land cover units between 2017 and 2024 is pre-

sented in Table 11. Positive values indicate an increase in area, while negative values indicate a decrease in land cover unit area. Indeed, classes such as dense forest, open forest, and water have experienced a considerable decrease in area, reflected in respective overall rates of change of −26.15%, −18.14%, and −37.54%, to the benefit of the classes wooded savanna (20.02%), cultivated land (0.62%), built-up/bare land (22.49%), and gold mining site (117.66%).

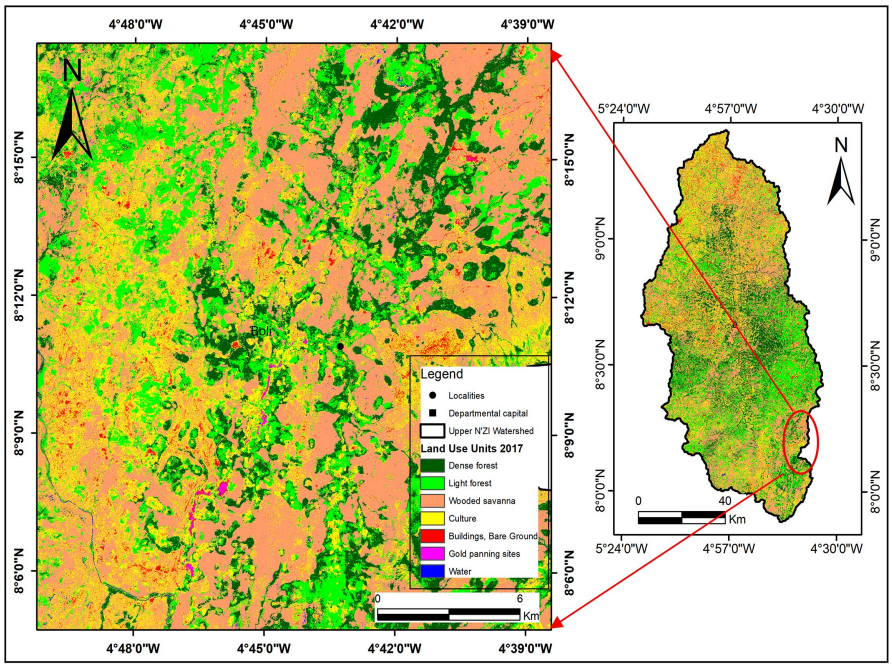


Figure 7. Land use in 2017 in the southeastern part of the BVHN.

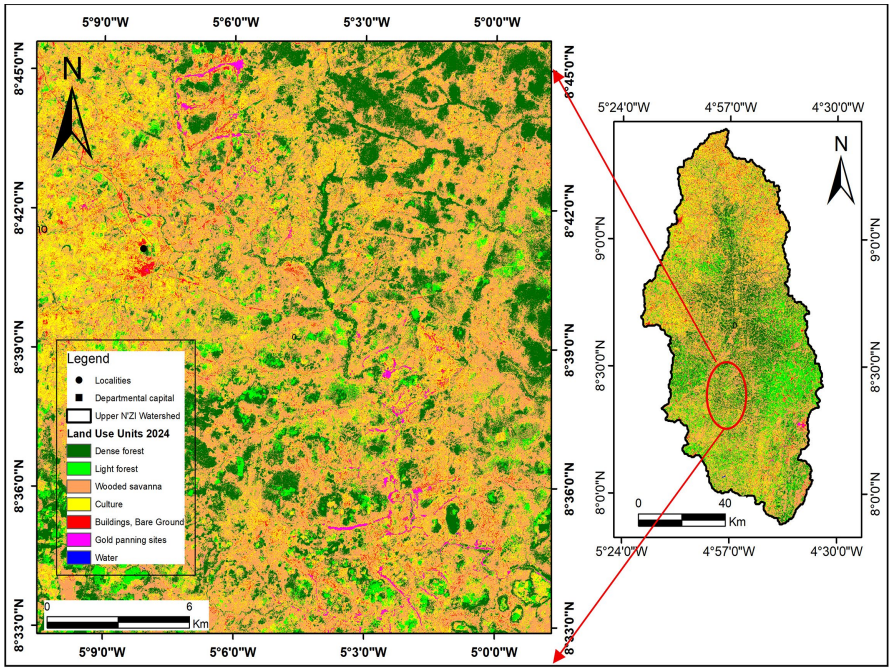


Figure 8. Land use in 2024, central-western BVHN.

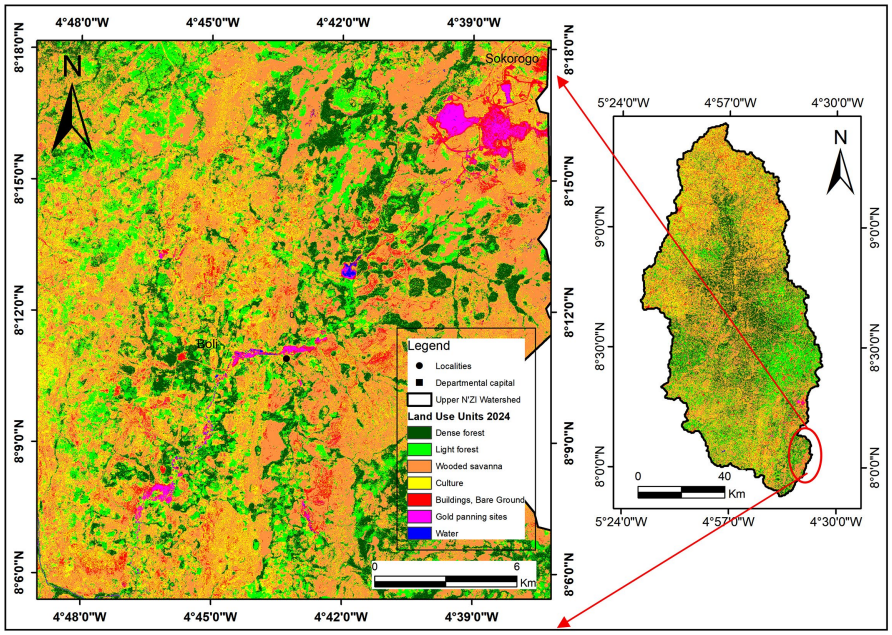


Figure 9. Land use in 2024, southeast BVHN.

Table 11. Statistical variation in class sizes from 2017 to 2024.

Classes	Variation (km²)	T (%)	TG (%)
Dense Forest	−409.80	−4.33	−26.15
Open Forest	−313.07	−2.86	−18.14
Wooded savanna	+649.88	+2.61	+20.02
Culture	+12.31	+0.09	+0.62
Built-up Area/Bare Soil	+49.24	+2.90	+22.49
Gold Panning Sites	+17.59	+11.11	+117.66
Water	−7.59	−6.72	−37.54

4.3. Analysis of the Origin of New Artisanal Gold Mining Sites Using a Post-Classification Comparison Approach

A specific analysis of land-cover units presents in 2017 that were converted to the "artisanal mining site" class by 2024 is presented in Table 12 below. The data shows that all land-cover classes contributed to the expansion of mining sites between 2017 and 2024 within the BVHN area. However, the proportions of this contribution vary by class, following the descending order shown here. Leading the list is the wooded savanna class, accounting for 39.83% (7.01 km²), followed by the cultivated land class at 24.11% (4.24 km²) and the built-up areas and bare soil class at 20.96% (3.69 km²). Next come the open forest and dense forest classes, with contributions of 7.76% (1.36 km²) and 6.20% (1.09 km²), respectively. Finally, the water class shows the lowest contribution at 1.14%

(0.20 km²).

Table 12. Origins of the expansion of artisanal gold mining sites between 2017 and 2024.

Class 2017	Proportion of conversion into artisanal gold mining sites in 2024	
	km²	%
Dense Forest	1.09	6.20
Open Forest	1.36	7.76
Wooded savanna	7.01	39.83
Culture	4.24	24.11
Built-up Area/Bare Soil	3.69	20.96
Water	0.20	1.14
Total	17.59	100

4.4. Impact of Land Cover Units on Water Flow

Analysis of the water retention coefficient of the different land cover classes in the study area reveals variability throughout the observed period. The results of this analysis are presented in Table 13.

Table 13. Retention coefficient for different land-use categories.

Years	C_r BVHN	C_r Dense Forest	C_r Open Forest	C_r Wooded savanna	C_r Culture	C_r Built-up Area/Bare Soil	C_r Gold Panning Sites
2017	134.63	35.64	39.24	36.92	22.75	0.00	0.085
2024	125.82	26.32	32.12	44.31	22.89	0.00	0.185

An examination of the water retention capacity index (Cr) values in the table above reveals two main trends: a progressive decline in water retention capacity for the "dense forest" and "open forest" classes dropping from 35.64 in 2017 to 26.32 in 2024 and from 39.24 in 2017 to 32.12 in 2024, respectively while other classes showed an increase. Notably, the "wooded savanna" class rose from 36.92 in 2017 to 44.31 in 2024. The "cropland" class went from 22.75 in 2017 to 22.89 in 2024, and the "artisanal gold mining site" class increased from 0.085 in 2017 to 0.185 in 2024. The chart in Figure 10 illustrates this trend across the various land-cover units between 2017 and 2024. Furthermore, at the watershed scale, the water retention coefficient experienced a slight decline between 2017 and 2024, falling from 134.63 to 125.82; overall, however, the value remained above 100, the threshold for watersheds with low levels of human impact.

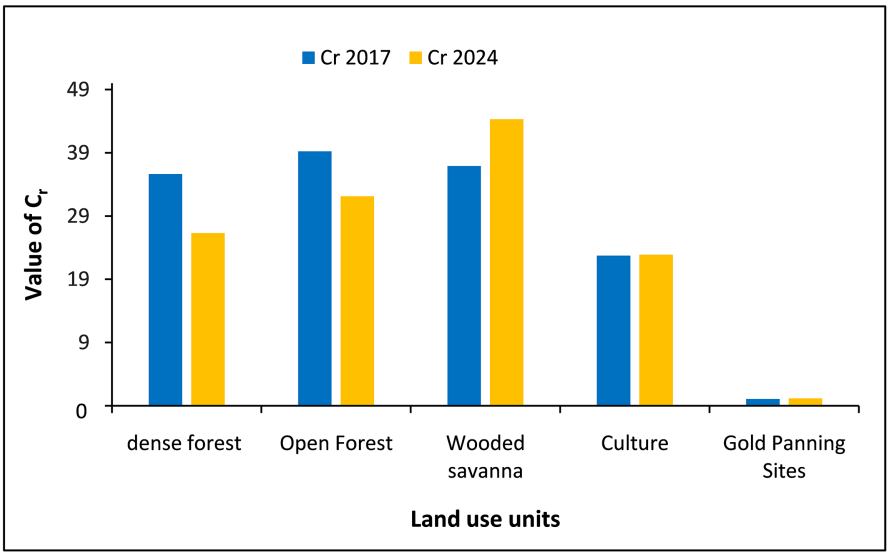


Figure 10. Changes in the retention coefficient for different land use categories.

4.5. Discussions

Remote sensing mapping of land cover changes using Sentinel-2 imagery has provided insight into the landscape covering the BVHN from 2017 to 2024. However, before analyzing the results, it is crucial to assess their accuracy to ensure they meet the user's needs and requirements [20] [29] [31]. In this study, the methodological approach to evaluating the authenticity of the results involved calculating several statistical parameters. The confusion matrices for the two classifications reveal some slight overlap between certain classes. According to [38], the difficulty in distinguishing between classes may be due to similar spectral signatures. More specifically, the gold panning site class exhibits a double confusion, one with the built-up area/bare soil class and the other with the water class. The first can be attributed to the presence of facilities built by gold panners for ore processing, sometimes even used as dormitories at the various mining sites. The second could be explained by the presence of muddy water reservoirs created by gold panners within the sites for washing ore, and pits left behind after extraction that fill with rainwater or water from the nearest stream. The highest level of confusion recorded in this study is 2.13%, observed between the wooded savanna and cultivated land classes for the 2017 classification. Overall, the confusion rates between the different classes show slight decreases from 2017 to 2024 and are all below 2.5%. However, these confounding errors do not in any way affect the study's results, as all confounding values are well below 70%, which is considered the threshold value [42]. Furthermore, the overall accuracy values obtained from this classification are 89.96% for 2017 and 87.17% for 2024. The Kappa coefficients are 0.86 for 2017 and 0.84 for 2024. According to the Kappa coefficient categorization work of [31], values between 0.81 and 1 are considered excellent, therefore the results of this study can be used with confidence.

The evaluation of the dynamics of the seven land cover units included in this

study revealed two trends. Initially, the regression of natural classes, namely the dense forest class which experienced a regression of −41.56% or −155.24 km^2, as well as the open forest class which experienced a regression of −9.91% or −717.16 km^2, according to the calculation of the overall evaluation rate over the period from 2017 to 2024, in favor of other classes known to have strong anthropogenic influences. Secondly, the area of wooded savanna increased by 14.76% (501.28 km^2), cultivated land by 0.61% (12.26 km^2), Built-up Area/Bare Soil by 22.19% (48.65 km^2), and gold panning sites saw the largest increase (120.17%, or 17.99 km^2), according to the overall rate of change. This phenomenon, observed nationally and particularly in the BVHN, is due to a combination of factors. The conversion of forests into agricultural land, primarily for export and food crops. The overexploitation of forest resources through timber sales and its use in construction and building furnishings. The production of charcoal and firewood. Rapid population growth and infrastructure development are factors accelerating the degradation of vegetation cover in the study area. This is compounded by the rampant and abusive practice of artisanal gold mining. Given the precarious living conditions of the rural population, most resort to gold panning as a means of survival, the only reliable way to earn a living, as demonstrated by the authors [43]-[45]. Indeed, gold panning is practiced not only by local populations but also by nationals from neighboring countries, sometimes in collusion with traditional authorities, thus rendering state-led repressive actions ineffective. This is evidenced by the rapid relocation of gold panners to new sites following evictions by law enforcement. One of the most significant causes of the proliferation of gold panning sites is the rise in the global price of gold per kilogram. Consequently, a post-classification comparison between the 2017 and 2024 land-cover maps was conducted to identify the spatial origins of new artisanal gold mining areas within the Upper N'ZI watershed (BVHN). The results indicated that all land-cover classes contributed to the expansion of mining sites, albeit to varying degrees, with the wooded savanna (39.83%) and cropland (24.11%) classes predominating. These findings align with the dynamics documented by [46], who quantified the conversion of 0.89 km^2 of land into artisanal mining sites in the Kokumbo area of Côte d'Ivoire between 2013 and 2023 including 0.40 km^2 of savanna and 0.21 km^2 of agricultural land thereby confirming that artisanal mining preferentially targets less protected areas. The significant contribution of cropland (24.11%) echoes observations made by [47] regarding land-use conflicts and food insecurity driven by artisanal mining in Burkina Faso. Furthermore, although the conversion of forest areas remained low (13.96%), [46] measured mercury concentrations reaching 20.4 mg/kg in Kokumbo sediments, revealing a risk of diffuse pollution even where the spatial footprint of mining is limited.

The impact of land-use unit dynamics on surface runoff in the BVHN was assessed by calculating the water retention coefficient [48]. This study highlights an area heavily impacted by human activity. Indeed, all C_r values for the different classes are below 100 ($C_r < 100$), with those for the gold panning site class ap-

proaching zero. In fact, the work of [37] shows that when C_r values are below 100, the area is considered highly degraded by human activity, characterized by low retention capacity and thus favoring surface runoff. Numerous studies, such as those by [37] in the Lakes District, [38] in the Divo Department, and [40] in the Aghein Lagoon watershed in Côte d'Ivoire, have reached the same conclusion. In reality, according to these studies, when C_r is low ($C_r < 100$), the area is dominated by erosion series, thus reducing the water infiltration capacity and consequently potentially affecting the groundwater availability of the area [49].

5. Conclusion

The objective of this study was to assess the dynamics of land-use units in the BVHN specifically artisanal gold mining sites and their impact on surface runoff between 2017 and 2024. To conduct this study, high-resolution (10 m) Sentinel-2 multispectral images processed on the Google Earth Engine (GEE) platform were used, employing the Random Forest (RF) machine learning algorithm via *JavaScript* programming. The results revealed a decrease in dense forest, open forest, and water surface areas, alongside an increase in wooded savanna, cropland, and built-up/bare soil areas. Notably, the area covered by artisanal gold mining sites expanded from 14.95 km^2 in 2017 to 32.92 km^2 in 2024, representing an overall growth rate of 117.66%. Post-classification change analysis highlighted significant conversion of wooded savanna and cropland into mining sites, followed by changes in the built-up/bare soil, open forest, dense forest, and water categories during the 2017-2024 period. Furthermore, water retention coefficients exceeding 100 ($C_r > 100$) indicate a low level of human-induced landscape alteration (anthropization) in the BVHN. However, C_r values showed a slight decline over the study period dropping from 134.63 in 2017 to 125.82 in 2024 likely driven by the expansion of unregulated artisanal gold mining; this trend exacerbates soil erosion and reduces infiltration, potentially diminishing groundwater availability.

Author Contributions

BENE Yao Amonkonan Jean-Philippe: study design, methodology development, fieldwork, data processing and analysis, and manuscript drafting. AHOUSSI Kouassi Ernest: scientific supervision and study coordination. YAO Kouassi Serge Aristide and Yapo Armand Patrick: critical review and contribution to the improvement of the manuscript. All authors have read and approved the published version of the manuscript.

Conflicts of Interest

The authors declare no conflicts of interest regarding the publication of this paper.

References

[1] Niangoran-Bouah, G. (1978) Idéologie de l'or chez les Akan de Côte d'Ivoire et du Ghana. *Journal des africanistes*, **48**, 127-140. https://doi.org/10.3406/jafr.1978.1808

[2] Denis, G. (2016) L'exploitation artisanale de L'or en Côte d'ivoire: La persistance d'une activité illégale. *European Scientific Journal*, *ESJ*, **12**, 18-36. https://doi.org/10.19044/esj.2016.v12n3p18

[3] COGINTA (2023) Étude qualitative spatio-socio-sécuritaire liée à l'orpaillage illégal dans le département de TENGRÉLA, Côte d'Ivoire. 108 p. http://www.coginta.org

[4] Soko, C. (2019) L'économie minière de l'orpaillage artisanal dans les sociétés post-conflit: Jeux des acteurs et enjeux de développement et de coopération in-ternationale. Étude de cas en Côte d'Ivoire. *Revue Organisations & territoires*, **28**, 61-79. https://doi.org/10.1522/revueot.v28n1.1023

[5] Kouadio, A.R.E., Bouah, E.F., Yao, S.S. and N'douba, V. (2022) Impact de l'exploitation aurifère artisanale et clandestine sur la distribution des Monogènes parasites branchiaux de Clarias gariepinus dans la rivière Bagoué (Côte d'Ivoire). *Revue Marocaine des Sciences Agronomiques et Vétérinaires*, **10**, 608-614. https://www.agrimaroc.org/index.php/Actes_IAVH2

[6] Atteyoub, M.H., Dit, M.S. and Mamadou, C. (2020) Impact socioec-onomique de l'orpaillage dans le cercle de kadiolo au mali. *Revue Malienne de Science et de Technologie*, **1**, 1987-1031. https://revues.ml/index.php/rmst/article/view/1944

[7] Affessi, A.S., Koffi, K.G.J.-C. and Sangare, M. (2016) Impacts sociaux et environnementaux de l'orpaillage sur les populations de la region du bounkani (Cote d'ivoire). *European Scientific Journal*, **12**, 288-306. https://doi.org/10.19044/esj.2016.v12n26p288

[8] Bamba, O., Pelede, S., Sako, A., Kagambega, N. and Miningou, M.Y.W. (2013) Impact de l'artisanat minier sur les sols d'un environnement agricole amenage au Burkina Faso. *Journal des Sciences*, **13**, 1-11. https://www.researchgate.net/publication/272229121_IMPACT_DE_L'ARTISANAT_MINIER_SUR_LES_SOLS_D'UN_ENVIRONNEMENT_AGRICOLE_AMENAGE_AU_BURKINA_FASO

[9] Andriamasinoro, F. and Angel, J. (2012) Artisanal and Small-Scale Gold Mining in Burkina Faso: Suggestion of Multi-Agent Methodology as a Complementary Support in Elaborating a Policy. *Resources Policy*, **37**, 385-396. https://doi.org/10.1016/j.resourpol.2012.04.004

[10] Kienon-Kabore, T.H., Bouadi, K.R., Yeo, A. and Tui, L.L. (2025) Recherches archéologiques dans les localités d'Ahouaty, N'dénou et Singrobo (centre de la Côte d'Ivoire): Contexte, bilan et perspectives. *European Scientific Journal*, *ESJ*, **21**, Article 185. https://doi.org/10.19044/esj.2025.v21n17p185

[11] Kouassi, A.M., Nassa, R.A., Bi, T.M.N.G., Kouame, K.F., Biemi, J. and Case, A. (2018) Caracterisation des debits d'etiage dans un contexte de changements climatiques: Cas du bassin versant du N'zi (Côte d'Ivoire). *Agronomie Africaine*, **30**, 215-223. https://www.ajol.info/index.php/aga/article/download/181808/171194

[12] Kouassi, A.M., Karim Nassa, R.A., N'guessan, T.M., Kouame, K.F. and Biemi J. (2018) Caractérisation des débits d'étiage dans un contexte de change-ments climatiques: Cas du bassin versant du N'ZI (Cote d'Ivoire). *Agronomie Africaine*, **30**, 215-223.

[13] Monnier, Y. (1978) Les sols. In: Vennetier, P., Ed., *Atlas de la Côte d'Ivoire*, Editions J.A., 20-21.

[14] Rouse Jr., J.W., Haas, R.H., Deering, D.W., Schell, J.A. and Harlan J.C. (1974) Monitoring the Vernal Advancement and Retrogradation (Green Wave Effect) of Natural Vegetation. NASA/GSFC Type III Final Report, 371 p.

[15] Huete, A.R. (1988) A Soil-Adjusted Vegetation Index (Savi). *Remote Sensing of En-*

vironment, **25**, 295-309. https://doi.org/10.1016/0034-4257(88)90106-x

[16] Tchibozo, E.A. and Toundoh, O.P. (2014) Détection localisée des zones dé-gradées de végétation par télédétection: Application à la zone de transition entre le bassin sédimentaire et le socle cristallin (Centre-Bénin). *International Journal of Innovation and Scientific Research*, **11**, 477-493. https://www.researchgate.net/publication/273768798_Detection_localisee_des_zones_d-gradees_de_vegetation_par_teledetection_application_a_la_zone_de_transition_entre_le_bassin_sedimentaire_et_le_socle_cristallin_Centre_-_Benin

[17] Gherraz, H. and Alkama, D. (2020) L'estimation de l'impact des espaces verts et des surfaces d'eau sur le climat urbain et la température de surface du sol (MILA, ALGÉRIE). *Revue Roumaine de Géographie*, **64**, 155-174. https://www.rjgeo.ro/issues/revue%20roumaine%2064_2/gherraz,%20alkama.pdf

[18] Giovos, R., Tassopoulos, D., Kalivas, D., Lougkos, N. and Priovolou, A. (2021) Remote Sensing Vegetation Indices in Viticulture: A Critical Review. *Agriculture*, **11**, Article 457. https://doi.org/10.3390/agriculture11050457

[19] Mihailescu, D. and Cimpeanu, S.M. (2023) Monitoring the Vegetation State in Oltenia Plain, Using Copernicus Land Products. *Environmental Engineering*, **11**, 458-466. https://landreclamationjournal.usamv.ro/pdf/2023/Art57.pdf

[20] Njeugeut, M.A.C., Youan, T.M., Kamenan, S.J.-R., Kouame, K.A., As-Soma, T.V. and Jourda, J.P. (2023) Cartographie des unités d'occupation du sol du District d'Abidjan depuis le cloud Google Earth Engine, sur la base des images optiques Sentinel-2 et des algorithmes de Machine Learning. *International Journal of Innovation and Applied Studies*, **40**, 310-332. https://www.researchgate.net/publication/372413317_Cartographie_des_unites_d'occupa-tion_du_sol_du_District_d'Abidjan_depuis_le_cloud_Google_Earth_Engine_sur_la_base_des_images_optiques_Sentinel-2_et_des_algorithmes_de_Machine_Learning_Mapping_of_land_

[21] Adetona, L., Agoïnon, N. and Vodounou, K.J.B. (2024) Disponibilité des eaux de surface pour l'élevage pastoral dans le bassin versant du Zou à l'exutoire de Domé (Bénin). *EWASH & TI Journal*, **8**, 1147-1156.

[22] Lemenkova, P. (2024) Exploitation d'images satellitaires Landsat de la région du Cap (Afrique du Sud) pour le calcul et la cartographie d'indices de végétation à l'aide du logiciel GRASS GIS. *Physio-Géo*, **20**, 113-129. https://doi.org/10.4000/11pyj

[23] Immitzer, M., Vuolo, F. and Atzberger, C. (2016) First Experience with Sentinel-2 Data for Crop and Tree Species Classifications in Central Europe. *Remote Sensing*, **8**, Article 166. https://doi.org/10.3390/rs8030166

[24] Wang, Q., Shi, W., Li, Z. and Atkinson, P.M. (2016) Fusion of Sentinel-2 Images. *Remote Sensing of Environment*, **187**, 241-252. https://doi.org/10.1016/j.rse.2016.10.030

[25] Ma, L., Cheng, L., Li, M., Liu, Y. and Ma, X. (2015) Training Set Size, Scale, and Features in Geographic Object-Based Image Analysis of Very High Resolution Unmanned Aerial Vehicle Imagery. *ISPRS Journal of Photogrammetry and Remote Sensing*, **102**, 14-27. https://doi.org/10.1016/j.isprsjprs.2014.12.026

[26] Amini, S., Saber, M., Rabiei-Dastjerdi, H. and Homayouni, S. (2022) Urban Land Use and Land Cover Change Analysis Using Random Forest Classification of Landsat Time Series. *Remote Sensing*, **14**, Article 2654. https://doi.org/10.3390/rs14112654

[27] Svoboda, J., Štych, P., Laštovička, J., Paluba, D. and Kobliuk, N. (2022) Random For-

est Classification of Land Use, Land-Use Change and Forestry (LULUCF) Using Sentinel-2 Data—A Case Study of Czechia. *Remote Sensing*, **14**, Article 1189. https://doi.org/10.3390/rs14051189

[28] Badda, H., Cherif, E.K., Boulaassal, H., Wahbi, M., Yazidi Alaoui, O., Maatouk, M., *et al*. (2023) Improving the Accuracy of Random Forest Classifier for Identifying Burned Areas in the Tangier-Tetouan-Al Hoceima Region Using Google Earth Engine. *Remote Sensing*, **15**, Article 4226. https://doi.org/10.3390/rs15174226

[29] Ouchra, H., Belangour, A. and Erraissi, A. (2023) Machine Learning Algorithms for Satellite Image Classification Using Google Earth Engine and Landsat Satellite Data: Morocco Case Study. *IEEE Access*, **11**, 71127-71142. https://doi.org/10.1109/access.2023.3293828

[30] Foody, G.M. (2002) Status of Land Cover Classification Accuracy Assessment. *Remote Sensing of Environment*, **80**, 185-201. https://doi.org/10.1016/s0034-4257(01)00295-4

[31] Chalifoux, S., Nastev, M., Lamontagne, C. and Latifovic, R. (2006) Car-tographie de l'occupation et de l'utilisation du sol par imagerie satellitaire Landsat en hydrogéologie. *Télédétection*, **6**, 9-17.

[32] Bergeri, I., Michel, R. and Boutin, J.-P. (2002) Technique pour tout savoir ou presque sur le coefficient kappa. *Médecine Tropicale*, **62**, 634-636. https://www.researchgate.net/publication/237658832_POUR_TOUT_SAVOIR_OU_PRESQUE_SUR_LE_COEFFICIENT_KAPPA

[33] Bernier, B. (1992) Introduction à la macroéconomie. Dunod, 217 p.

[34] Singh, A. (1989) Review Article Digital Change Detection Techniques Using Remotely-Sensed Data. *International Journal of Remote Sensing*, **10**, 989-1003. https://doi.org/10.1080/01431168908903939

[35] Badjana, H.M., Helmschrot, J., Selsam, P., Wala, K., Flügel, W., Afouda, A., *et al*. (2015) Land Cover Changes Assessment Using Object-Based Image Analysis in the Binah River Watershed (Togo and Benin). *Earth and Space Science*, **2**, 403-416. https://doi.org/10.1002/2014ea000083

[36] Provencher-Nolet, L., Bernier, M. and Lévesque, E. (2014) Quantification des changements récents à l'écotone forêt-toundra à partir de l'analyse numérique de photographies aériennes. *Écoscience*, **21**, 419-433. https://doi.org/10.2980/21-(3-4)-3715

[37] Cecchi, P., Gourdin, F., Koné, S., Corbin, D., Etienne, J. and Casenave, A. (2009) Les petits barrages du nord de la Côte d'Ivoire: Inventaire et potentialités hydrologiques. *Sécheresse*, **20**, 112-122. https://doi.org/10.1684/sec.2009.0164

[38] Soro, G. (2010) Évaluation quantitative et qualitative des ressources en eau sou-terraines dans la région des lacs (Centre de la Côte d'Ivoire): Hydrogéologie et hydrochimie des aquifères discontinus du district de Yamoussoukro et du dépar-tement de Tiebissou. Thèse de Doctorat, Université de Cocody-Abidjan, 254 p.

[39] Soro, G., Ahoussi, K.E., Kouadio, K.E., Soro, T.D., Oulare, S., Saley, M.N., Soro, N. and Biemi, J. (2014) Apport de la télédétection à la cartographie de l'évolution spatio-temporelle de la dynamique de l'occupation du sol dans la région des Lacs (Centre de la Côte d'Ivoire). *Afrique Science*, **10**, 146-160.

[40] Seydou, D., Dabissi, N., Armand, T.B.Z., Amidou, D., Bamory, K., Rose, E.K., *et al*. (2018) Effets de la dynamique du couvert végétal sur les écoulements dans le bassin ver-sant de la lagune aghien en Côte d'Ivoire. *European Scientific Journal*, **14**, 312-332. https://doi.org/10.19044/esj.2018.v14n36p312

[41] Yao, K.S.A. (2022) Apport de l'hydrochimie et de la géochimie environnementale

dans l'évaluation des ressources en eau des environnements miniers du départe-ment de Divo (Sud-ouest de la Côte d'Ivoire). Thèse de Doctorat, Université Félix Houphouët Boigny de Cocody, 293 p.

[42] Mama, V.J. and Oloukoi, J. (2003) Evaluation de la précision des traitements analogiques des images satellitaires dans l'étude de la dynamique de l'occupation du sol. *Télédétection*, **3**, 429-441. https://www.researchgate.net/publication/325120156_EVALUATION_DE_LA_PRECI-SI-ON_DES_TRAITEMENTS_ANALOGIQUES_DES_IMAGES_SATELLITAIRES_DANS_L'ETUDE_DE_LA_DYNAMIQUE_DE_L'OCCUPATION_DU_SOL

[43] Kitula, A.G.N. (2006) The Environmental and Socio-Economic Impacts of Mining on Local Livelihoods in Tanzania: A Case Study of Geita District. *Journal of Cleaner Production*, **14**, 405-414. https://doi.org/10.1016/j.jclepro.2004.01.012

[44] Dondeyne, S., Ndunguru, E., Rafael, P. and Bannerman, J. (2009) Artisanal Mining in Central Mozambique: Policy and Environmental Issues of Concern. *Resources Policy*, **34**, 45-50. https://doi.org/10.1016/j.resourpol.2008.11.001

[45] Traoré, A.B. (2022) Impact socioéconomique de l'orpaillage dans le cercle de Kéniéba au Mali. *International Journal of Accounting, Finance, Auditing, Management and Economics*, **3**, 251-268.

[46] Kouadio, K.B., Resongles, E., Ahoussi, K.E., Ouattara, Z., Konaté, I., Fayol, N., *et al*. (2025) Environmental Contamination by Metals, Metalloids, and Cyanides in the Historic and Active ASGM Area of Kokumbo in Côte d'ivoire. *Environmental Science and Pollution Research*, **32**, 13699-13725. https://doi.org/10.1007/s11356-025-36403-6

[47] Sangli, G., Ouattara, B., Ouedraogo, M. and Azianu, K.A. (2022) Des pratiques agricoles aux activités minières: L'orpaillage et l'insécurité alimentaire au Burkina Faso. *Revue de Géographie de l'Université de Ouagadougou*, **11**, 50-60. https://hal.science/hal-05222463v1

[48] Robin, P.-R. (2023) Effets du développement et de la transformation de l'orpaillage sur les dynamiques foncières en Guinée. Comité Technique "Foncier et développement". AFD-MEAE, 124 p. https://hal.science/hal-04572379v1

[49] Hue, B.B.F., Kambire, B. and Alla, D.A. (2020) Mutations environnementales liées à l'orpaillage à Ity (Ouest de la Côte d'Ivoire). *Annales de l'Université de Moundou*, **7**, 2707-6830. https://aflash-revue-mdou.org/article/192/pdf